



Onshore sandbar migration at Tairua Beach (New Zealand): Numerical simulations and field measurements

B. van Maanen^{a,b,*}, P.J. de Ruiter^a, Giovanni Coco^b, K.R. Bryan^c, B.G. Ruessink^a

^a Department of Physical Geography, Faculty of Geosciences, Institute for Marine and Atmospheric Research, Utrecht University, PO Box 80-115, 3508 TC Utrecht, The Netherlands

^b National Institute of Water & Atmospheric Research, PO Box 11-115, Hamilton 3216, New Zealand

^c Department of Earth and Ocean Sciences, University of Waikato, Private Bag 3105, Hamilton 3240, New Zealand

ARTICLE INFO

Article history:

Received 29 January 2008

Received in revised form 8 May 2008

Accepted 11 May 2008

Keywords:

nearshore sandbars
sediment transport
onshore migration
surf zone bores
wave skewness

ABSTRACT

We observed the onshore migration (3.5 m/day) of a nearshore sandbar at Tairua Beach, New Zealand during 4 days of low-energy wave conditions. The morphological observations, together with concurrent measurements of waves and suspended sediment concentrations, were used to test a coupled, wave-averaged, cross-shore model. Because of the coarse bed material and the relatively low-energy conditions, the contribution of the suspended transport to the total transport was predicted and observed to be negligible. The model predicted the bar to move onshore because of the feedback between near-bed wave skewness, bedload, and the sandbar under weakly to non-breaking conditions at high tide. The predicted bathymetric evolution contrasts, however, with the observations that the bar migrated onshore predominantly at low tide. Also, the model flattened the bar, while in the observations the sandbar retained its steep landward-facing flank. A comparison between available observations and numerical simulations suggests that onshore propagating surf zone bores in very shallow water (<0.25 m) may have been responsible for most of the observed bar behaviour. These processes are missing from the applied model and, given that the observed conditions can be considered typical of very shallow sandbars, highlight a priority for further field study and model development. The possibility that the excess water transported by the bores across the bar was channelled alongshore to near-by rip-channels further implies that traditional cross-shore measures to judge the applicability of a cross-shore morphodynamic model may be misleading.

© 2008 Elsevier B.V. All rights reserved.

1. Introduction

Subtidal sandbars characterize the subaqueous cross-shore profile of most micro- to mesotidal, wave-dominated beaches (Wijnberg and Kroon, 2002). During the last two to three decades, understanding the mechanisms driving cross-shore migration in response to time-varying offshore wave forcing has been one of the foci of field and laboratory experiments, and of numerical modeling. The processes responsible for offshore bar migration are relatively well understood. Alongshore-homogeneous offshore directed currents ('undertow') have been identified, especially under breaking-wave conditions, as the main driving mechanism for offshore sediment transport and, because of gradients therein, for offshore sandbar migration (Gallagher et al., 1998). However, the causes of shoreward directed sediment transport are not well known to date.

Over the years, a number of processes have been held responsible for onshore bar migration. These processes include wave skewness (preponderance of high crests; Plant et al., 2004; Hsu et al., 2006; Ruessink et al., 2007), wave asymmetry (steep front faces; Hoefel and Elgar, 2003), near-bed streaming (Trowbridge and Young, 1989), Stokes drift (Henderson et al., 2004), with other mechanisms, such as near-bed sediment-induced buoyancy (Falchetti et al., 2007), also of potential importance. Most of the listed studies used so-called non-coupled models, in which measured time series of near-bed flow were used to drive the sediment transport, without feedback from the evolving bathymetry to the flow. All non-coupled models have been tested only on the Duck94 data (Gallagher et al., 1998) and obtained similar skill, despite drastically different underlying sediment transport processes. This implies that the Duck94 dataset is essentially underdetermined; particularly, it is lacking detailed observations of the near-bed vertical structure of cross-shore flow and sediment concentration profiles across the sandbar. Recently, Ruessink et al. (2007) successfully modeled onshore and offshore nearshore sandbar migration events (including Duck94) with a coupled, wave-averaged, cross-shore model and concluded that the onshore bar movement is related to the feedback between near-bed wave skewness, bedload transport, and the sandbar. However, they also pointed to the need for

* Corresponding author. National Institute of Water & Atmospheric Research, PO Box 11-115, Hamilton 3216, New Zealand. Tel.: +64 7 8591858; fax: +64 7 8560151.

E-mail address: b.vanmaanen@niwa.co.nz (B. van Maanen).

near-bed observations of flow and sediment concentration to test their suggested mechanism for onshore bar migration.

Here we test Ruessink et al.'s (2007) model in a hindcast study of a 4-day onshore bar migration event observed at Tairua Beach, located on the east coast of the Coromandel Peninsula, North Island, New Zealand. We compare model predictions to measurements of waves, suspended sediment, and morphological change obtained under low-wave conditions.

2. Methodology

2.1. Model description

The applied model, described in detail in Ruessink et al. (2007), simulates the temporal evolution of cross-shore profiles using coupled, wave-averaged equations for cross-shore wave transformation, the vertical structure of cross-shore and alongshore flow, and sediment transport (suspended load and bedload). The model is initialized with a bed profile, a median grain size, time series of offshore wave parameters (height, period and direction) and water level.

The wave model consists of three first-order differential equations, (1) the energy balance equation for wave motion as formulated by Battjes and Janssen (1978), (2) the energy balance equation for the surface rollers on the breaking-wave crest (Nairn et al., 1990), and (3) the time-averaged and depth-integrated cross-shore momentum balance neglecting inertial effects and bed-shear stress to compute set-down and set-up. The output of the wave model feeds into the flow model of Reniers et al. (2004) to predict the vertical distribution of the cross-shore and alongshore flow.

The total sediment transport q_{tot} is obtained as the sum of the bedload q_{bed} and suspended load q_{sus} transport rates. The bedload transport rate is the time-average of an instantaneous rate (Van Rijn, 1995; Ribberink, 1998). The flow used to calculate this rate is derived from a time series of the intra-wave near-bottom horizontal velocity vector of the combined wave–current motion. This time series is constructed to have the same characteristics as a natural wave field, and comprises a group of seven short waves, the associated group-forced infragravity wave, and the mean flow estimated by the flow model at the lowest computation gridpoint (1 cm above the bed), \bar{u}_{ig} . The skewness of the short waves is estimated with Rienecker and Fenton's (1981) stream function theory; the model ignores wave asymmetry. With \bar{u}_{ig} , the contribution of the mean flow in the wave bottom boundary layer to the bedload is considered. Its cross-shore component, \bar{u}_{igx} , is generally onshore directed under low, non-breaking waves owing to streaming and offshore directed under surf zone conditions. The bedload equation also contains a term to stimulate gravity-induced downslope and to hinder gravity-induced upslope transport. The suspended sediment transport rate is defined as the integral of the product of the cross-shore mean flow and time-averaged sediment concentrations from the edge of the bedload layer to the water surface and follows the approach of Van Rijn (1993).

The computed cross-shore gradients in the total, depth-integrated sediment transport rate drive temporal bed elevation change from continuity, using a bed porosity of 0.4, on a 4-point implicit Preismann scheme. The bottom changes feed back onto the wave and current model at the next time step, thus forming a coupled set of equations.

2.2. Observations

We studied model performance using data collected during a field experiment conducted from 13 to 16 March 2001 at Tairua Beach, a 1.2-km long embayed beach located on the east coast of the Coromandel Peninsula on the North Island of New Zealand. The beach is classified as an intermediate beach (Bogle et al., 1999) based on the classification of beach types by Wright and Short (1984) and

frequently displays transverse-bar-rip morphology. The sediments at Tairua Beach are composed of coarse sand with a median diameter of 0.6 mm.

During the experiment a beach profile was repeatedly measured up to a depth of 7 m below mean sea level using an instrumented sea sled (Smith et al., 1997; Fig. 1a and b). The sled was towed seawards eight times by means of a boat and pulled onshore by a hydrostatically powered winch. A survey prism attached to the top of the sled's 12.75-m-high mast was used to determine seabed elevations every 0.1–0.2 m across the profile. Bathymetric data were corrected for shore-normal/parallel sled tilt using an inclinometer to give the position and elevation of the seabed directly below the sled mast. Measured bed elevation profiles show that the rate of onshore migration of the bar crest averaged 3.5 m/day (Fig. 2).

The net elevation change, Δ_{net} , and the root-mean-square elevation change, Δ_{rms} , between two consecutive measured bed profiles were calculated as

$$\Delta_{net} = \frac{1}{N_x} \sum_{i=1}^{N_x} \Delta_i \text{ and} \quad (1)$$

$$\Delta_{rms} = \sqrt{\frac{1}{N_x} \sum_{i=1}^{N_x} \Delta_i^2}, \quad (2)$$

respectively, where Δ_i is the change in measured bed elevation at cross-shore position i and N_x is the number of positions. In the computations of Eqs. (1) and (2), we only included the cross-shore locations in the range $-200 \leq x \leq -67$ m. This range includes the part of the profile that changed due to bar migration but excludes the intertidal beach zone. The net change is always at least about three

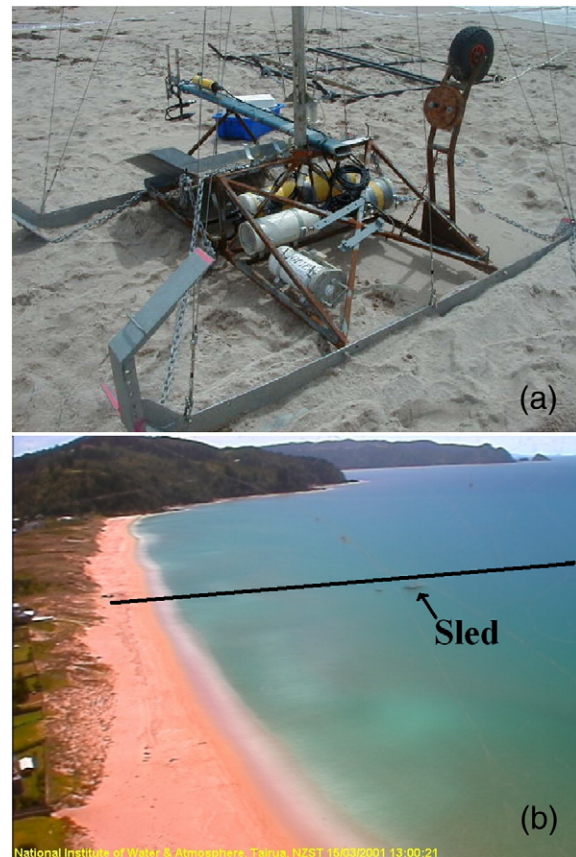


Fig. 1. (a) Instrumented sled used during the experiment at Tairua Beach. (b) Time-averaged video image of Tairua Beach during the experiment. Measurements were taken in the cross-shore transect as indicated by the black line.

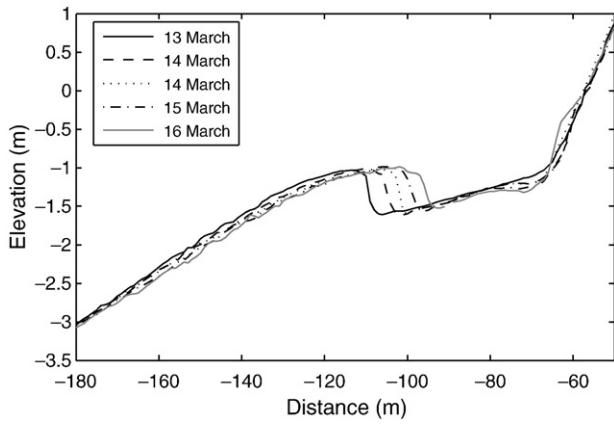


Fig. 2. Measured elevation versus cross-shore distance at Tairua Beach.

times smaller than the rms-change (Fig. 3), implying that, consistently with the approach of other authors (e.g. Gallagher et al., 1998; Ruessink et al., 2007; Ruessink and Kuriyama, 2008), the cross-shore sediment transport mechanisms must have dominated over gradients in the alongshore transport rates.

During the process of winching the sled shoreward, the sled was stopped at pre-arranged points to take stationary measurements of near-bed sediment concentrations and hydrodynamics. Suspended sediment concentrations were measured at 0.18 and 0.28 m above the bed using optical backscatter sensors mounted on a 2-m-long horizontal arm, which extended from the ‘up-drift’ side of the sled. An acoustic Doppler velocity meter, also mounted on the sled’s arm, burst-sampled flow velocities 0.18 m above the bed. A pressure sensor deployed about 900 m offshore in 10 m water depth provided the offshore data necessary to force the model. Every 4 h, this sensor measured the water pressure for 1 h at a sampling frequency of 2 Hz. As a result, values of the root-mean-square wave height H_{rms} and zero-crossing wave period T_{m02} were only available every 4 h (Fig. 4a and b). Tidal elevation data, also recorded in 10 m water depth, were available every 30 min (Fig. 4c). The field site was monitored by a video camera mounted at the south end of the beach (70.5 m above chart datum). The camera provided a snapshot (photograph) and a 10-min time-exposure image (e.g., Fig. 1b) every day-light hour.

As can be seen in Fig. 4, the offshore H_{rms} increased slowly from about 0.3 to 0.45 m during the experiment, with an associated drop in T_{m02} from about 10 to 7 s. The tide was semi-diurnal with an approximate 1.5 m range. The video images showed wave breaking on the bar to be limited to low-tide conditions.

2.3. Model set-up

The initial bed profile, used for the simulations, extended from the location where the offshore data had been collected to the dune foot.

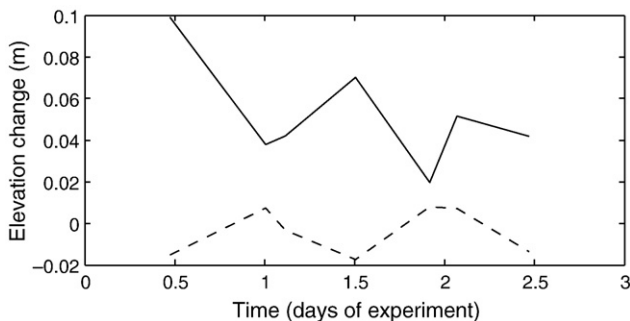


Fig. 3. Net (dashed line) and root-mean-square (solid line) elevation change during the experiment.

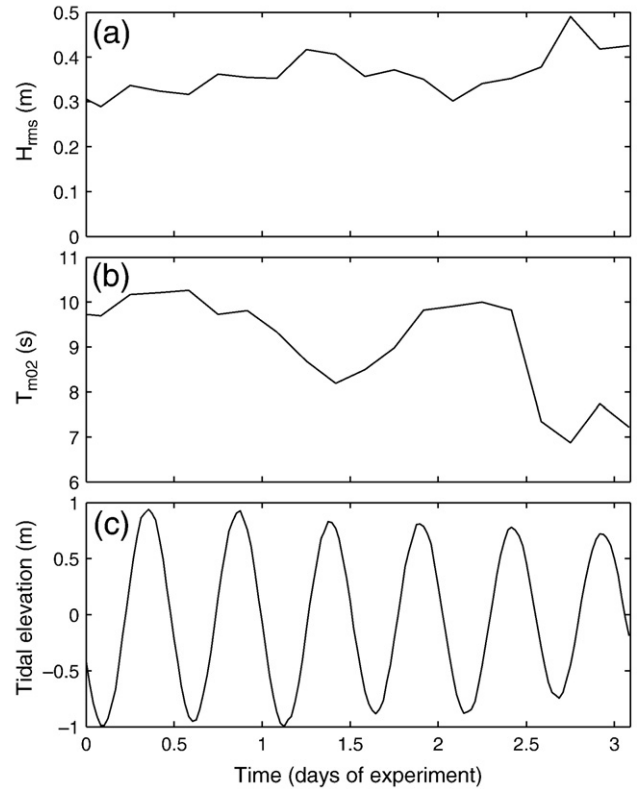


Fig. 4. Measured (a) offshore root-mean-square wave height H_{rms} , (b) offshore zero-crossing wave period T_{m02} , and (c) tidal elevation during the experiment.

In the deepest regions a grid size of 10 m was used. The grid size decreased with decreasing water depth to a minimum of 1 m on the intertidal beach. The initial bed level shoreward of $x = -69$ m, where sediment was coarser (unpublished data), was considered as a fixed layer where erosion cannot further decrease the bed elevation. The presence of a fixed layer avoided numerical instabilities developing close to the shoreline.

The model was forced with the time series of tidal elevation, wave height, and period as presented in Fig. 4. In all simulations, an offshore wave angle of 0° was assumed. This assumption seems to be valid considering the orientation of Tairua Beach. Moreover, Tairua Beach is a pocket beach where strong refraction causes the waves to approach the coast perpendicular to the general shoreline trend. Video images of the beach during the experiment also show the wave crests to be parallel to the shoreline. We return to the sensitivity of our results to the offshore wave angle in Section 3. Additional inputs include the wind direction and velocity, as obtained from NOAA/NCEP (Caplan et al., 1997). The numerical time step in all simulations was 30 min. The offshore wave parameters were interpolated linearly between the available observations.

At each time step, the model’s shoreward boundary was defined as the cross-shore location where the maximum relative wave period T_{dry} ,

$$T_{dry} = T_{m02} \sqrt{\frac{g}{h}} \tag{3}$$

exceeded 50 for the first time. Here, $g = 9.81 \text{ m/s}^2$ is gravitational acceleration and h is water depth. For example, if $T_{m02} = 8 \text{ s}$, no hydrodynamic and sediment transport computations were carried out in depths less than 0.25 m. This is not an uncommon feature of state-of-the-art numerical models describing surf zone morphodynamics (e.g. Garnier et al., 2006) which also lack a description of very shallow-

water processes, such as swash/backwash, and associated sediment transport rates.

2.4. Model calibration

As noted by Ruessink et al. (2007), the predictive capability of the model depends on the values of a number of free parameters. Here, the free parameters included in the wave model (a dissipation factor α and a wave height-to-depth ratio γ) were set to existing literature values. Where possible, we set values of free parameters in the flow and sediment transport equations to values determined from the observations. For instance, the parameter c_f (Ruessink et al., 2007) steers the magnitude of the offshore transport induced by bound infragravity waves. We did not find evidence for the presence of these flow motions in the data, and hence we set c_f to 0. We included three parameters in the model-calibration phase: the wave-delay parameter λ , the tangent of the angle-of-repose $\tan \phi$, and the current-related roughness $k_{s,c}$. The wave-delay parameter λ , introduced into the model by Roelvink et al. (1995), controls the magnitude of the maximum wave height in the Battjes and Janssen (1978) formulation. With an increase in λ , the precise location of wave breaking over the bar is shifted slightly in the onshore direction. In this way, λ also affects the location of maximum undertow and sediment transport rates. The tangent of the angle of repose, $\tan \phi$, controls the magnitude

of the gravity-induced bedload transport. A decrease in $\tan \phi$ hinders upslope transport and stimulates downslope transport, leading to a slightly less pronounced bar-trough relief. The current-related roughness $k_{s,c}$ affects the magnitude of the suspended load transport as it determines the lower depth of the integral of the product of cross-shore mean-current and time-averaged concentration. With an increase in $k_{s,c}$, the suspended transport rates decrease. Beforehand, the effect of these parameters on model performance was not known.

To find the optimum values for these three parameters, we ran the model 1000 times with parameter vectors chosen randomly from what we, based on earlier model experience, considered to be the feasible parameter space. The optimal combination of parameter values is the combination that produces the lowest squared-error, computed as

$$F = \sum_{x,t} (z_{\text{model}}(x, t) - z_{\text{meas}}(x, t))^2, \quad (4)$$

where z_{model} and z_{meas} are the modeled and measured bed elevations, respectively, and t represents the time steps at which the bed profiles are extracted. To calculate Eq. (4), the bed elevations at the same cross-shore locations were used as in the calculation of Eqs. (1) and (2). We found the optimum values to be $\lambda = 1.1$, $\tan \phi = 0.23$, and $k_{s,c} = 0.08$ m. The optimum values for λ and $\tan \phi$ are within the range of previously determined values (e.g., Ruessink et al., 2007). We return to the high value for $k_{s,c}$ in the next section.

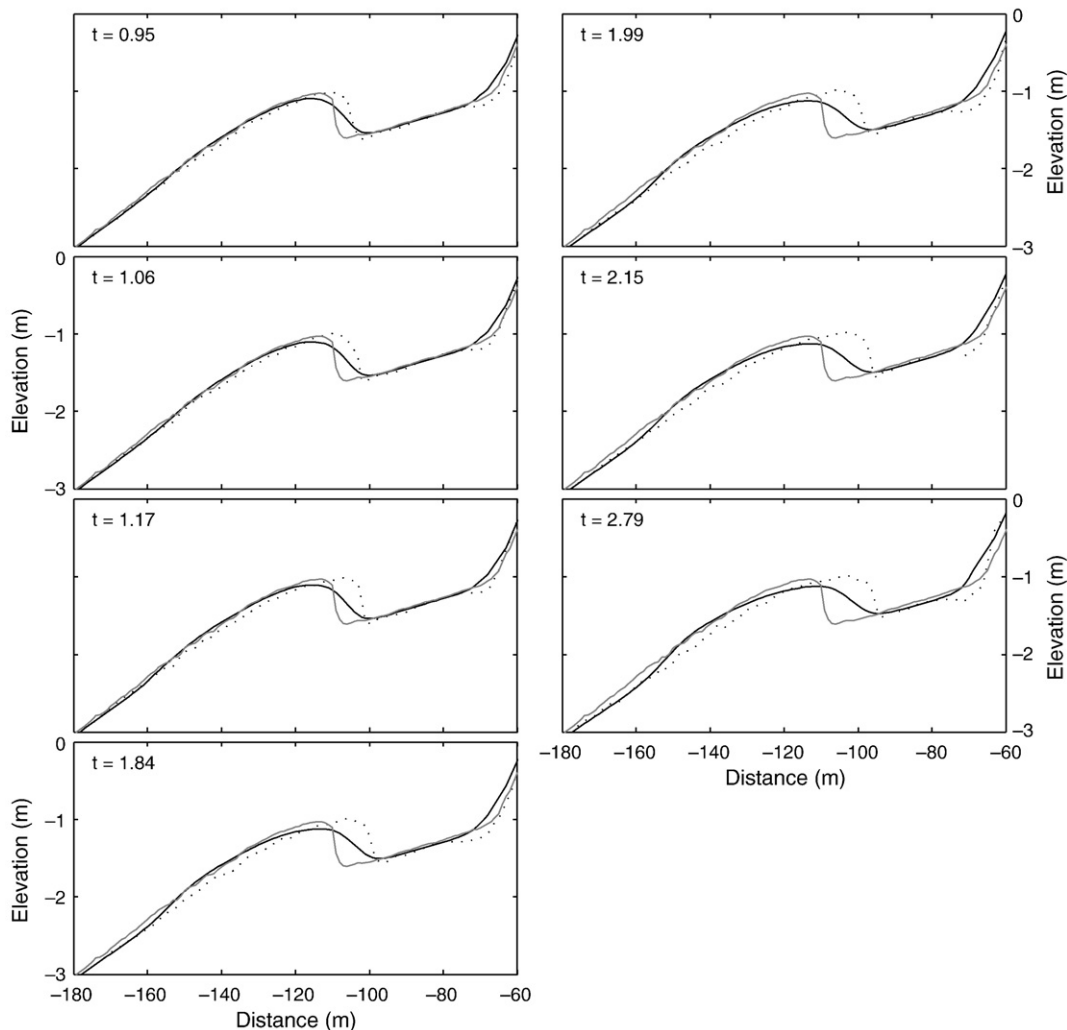


Fig. 5. Measured (dotted line), modeled (solid line), and initial (shaded line) bed elevation versus cross-shore distance. Time, noted on the top-left corner of each plot, is in days of the experiment.

3. Results

With the optimum parameter values, the model predicted onshore bar migration (Fig. 5). The skill S , defined as 1 minus the ratio of the cumulative squared prediction error to the cumulative squared no-change error,

$$S = 1 - \frac{\sum_{x,t} (z_{model}(x,t) - z_{meas}(x,t))^2}{\sum_{x,t} (z_{meas}(x,t) - z_{meas}(x,t = t_0))^2}, \quad (5)$$

where $z_{meas}(x,t=t_0)$ is the initial profile, was 0.56, indicating reasonably good model results. It is obvious from Fig. 5, however, that the model underpredicted the rate of onshore movement and failed to reproduce the evolution of the shape of the bar. The bar is predicted to flatten, reducing the height of the crest and the steepness of the onshore flank of the bar. The measured bed profiles show that this steepness is maintained during the field experiment. Because of the modeled flattening process, the bar crest is predicted to move offshore for the first half day of the experiment (Fig. 6a), which is not in agreement with the observations.

Fig. 6b shows the predicted wave height during the experiment for the cross-shore range $-250 \leq x \leq -50$ m. The wave height across the bar is tidally modulated. During low tide, enhanced wave breaking causes a decrease in wave height at the bar. At high tide, in contrast, the waves pass over the bar unaltered, whereas at mid tide the wave height at the bar is higher than offshore because of shoaling. The model stops the calculations at the seaward side of the bar crest at low tide during four tidal cycles (Fig. 6b) because the small water depths cause T_{dry} to exceed 50. The rather poor agreement between observations and numerical predictions of wave height (root-mean-square error amounted to 0.09 m) can be related to a number of factors including the limited ability of linear wave theory to predict the

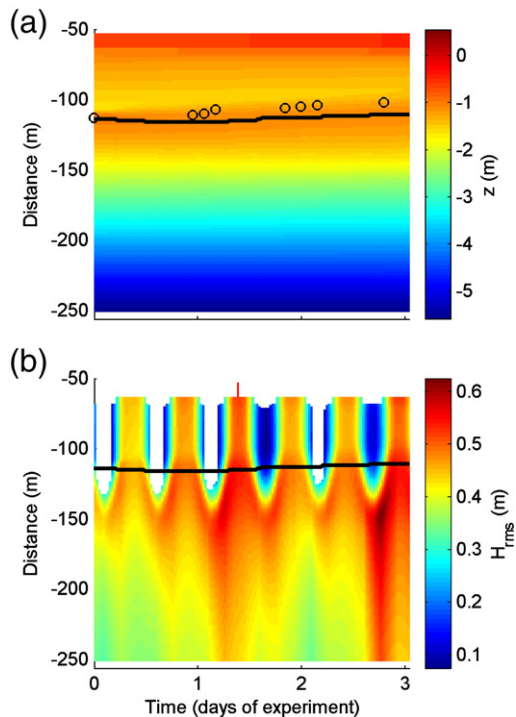


Fig. 6. Predicted (a) bed elevation z , and (b) root-mean-square wave height H_{rms} versus time. The black line and circles represent the predicted and measured sandbar crest location, respectively.

shoaling of long-period swell, poor estimation of frictional effects or even a mismatch between the sampling protocol of the onshore current meter (mounted on the sled and used for this comparison) and the offshore pressure sensor (placed in around 10 m water depth and used to force the model). Also, the numerical model has not been calibrated to fit wave characteristics.

The magnitude and sign of the bedload transport rates depend on the predicted magnitudes of the cross-shore mean current at 1 cm above the bed \bar{u}_{lgx} and the near-bed short-wave orbital motion u_{nl} . Under non-breaking waves, \bar{u}_{lgx} is onshore directed (<0.01 m/s) due to near-bed streaming (Fig. 7a), but becomes offshore directed with maximum values of about -0.03 m/s under breaking waves at low tide. Fig. 7b shows the predicted third-order short-wave moment $\langle |u_{nl}|^2 u_{nl} \rangle$. This third-order moment is not used in the present model, but it serves as a proxy to the effect of near-bed wave skewness on bedload transport. As is obvious from Fig. 7b, $\langle |u_{nl}|^2 u_{nl} \rangle$ values are strongly tidally modulated and close to the bar crest these values peak at mid tide as a result of shoaling. Fig. 8 shows that measured and predicted $\langle |u_{nl}|^2 u_{nl} \rangle$ were well related, with a systematic overprediction of the measured values by a factor of 2.5 (the model thus appears to overpredict wave skewness).

As is obvious from Fig. 9a, the bedload transport rates are offshore during wave breaking at low tide, but onshore otherwise. The largest onshore directed bedload transport rates are predicted around mid tide, when up to 30% of the waves are predicted to break, consistent with model results of the Duck94 experiment as found by Ruessink et al. (2007). This onshore directed transport is induced by the skewness of the near-bed orbital motion, as clearly displayed by the similarity between the $\langle |u_{nl}|^2 u_{nl} \rangle$ patterns in Fig. 7b and q_{bed} patterns in Fig. 9a.

The model predicts non-zero suspended sediment rates when the effective bed-shear stress exceeds the critical bed-shear stress, something which is almost never the case in the present model simulations. Therefore, the suspended sediment concentration is predicted to be 0 kg/m^3 for almost every cross-shore location at most time steps, resulting in no suspended sediment transport (Fig. 9b). Even for the two short periods of time, when intense wave breaking causes the critical bed-shear stress to be exceeded, the offshore directed suspended sediment transport is very small compared to the bedload transport. Thus, the predicted total sediment transport (Fig. 9c) is essentially equal to the bedload transport (compare to Fig. 9a). Suspended sediment concentration measurements performed at various cross-shore locations during the field experiment, however, show the presence of suspended material in the water. Because the model predicts a suspended sediment concentration of 0 kg/m^3 , the suspended sediment transport rate is underestimated. Time-averages of measured concentrations (instantaneous concentrations were generally correlated to wave orbital motions, not shown) were used to obtain vertical concentration profiles by computing the suspended sediment concentration for 800 elevations spaced linearly between the upper edge of the bedload layer (determined by the value of $k_{s,c}$) and the water surface, assuming the concentration to decay exponentially with height above the bed (Nielsen, 1979). Subsequently, depth integration of the product of these concentration profiles and associated modeled velocity profiles (interpolated for the same 800 elevations above the bed as used for the concentration profiles) provided sediment transport rates. These “measured” transport rates are, together with the predicted bedload transport, shown in Fig. 10a. At the most offshore located point where the sled stopped to obtain concentration measurements ($x \approx -350$ m), the suspended transport is relatively important compared to the modeled bedload transport ($|q_{sus}|/(|q_{sus}|+|q_{bed}|) \approx 0.8$; Fig. 10b). However, at this location the transport rates are low ($|q_{sus}|+|q_{bed}| < 4.5 \cdot 10^{-7} \text{ m}^2/\text{s}$). Closer to the bar crest ($x \approx -155$ m) where the transport rates are an order of magnitude higher ($|q_{sus}|+|q_{bed}| > 3.2 \cdot 10^{-6} \text{ m}^2/\text{s}$), the suspended transport rates are relatively less important ($|q_{sus}|/(|q_{sus}|+|q_{bed}|) \approx 0.07$), implying that the predicted zero suspended transport rates are not a crucial error. Concentration data are not available closer to the

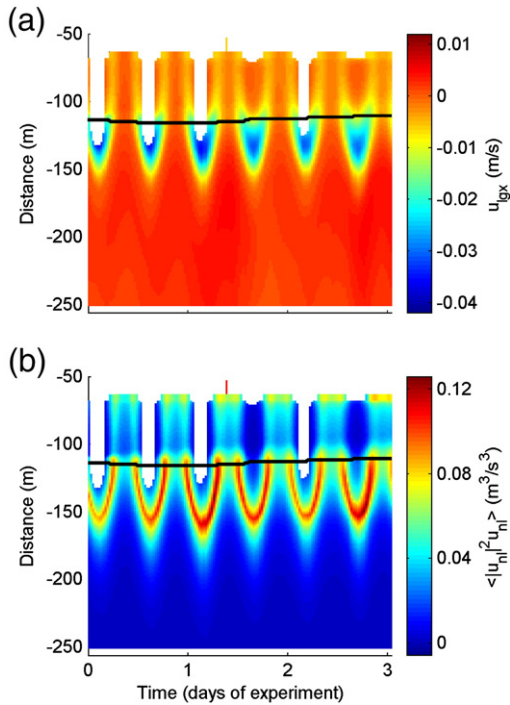


Fig. 7. Predicted (a) cross-shore mean current at 1 cm above the bed $\bar{u}_{lg,x}$ and (b) third-order short-wave moment $\langle |u_{ni}|^2 u_{ni} \rangle$ versus time. The black line represents the predicted sandbar crest location.

bar crest; however, the predicted mean flows at high tide across the bar are so low (predicted values for the depth-averaged cross-shore mean current are less than -0.05 m/s) that the suspended load transport rates would have been zero even if the waves had stirred sediment. It remains uncertain if suspended sediment transport is also negligible at low tide, when the model stops prematurely at the seaward side of the bar.

The unimportance of suspended sediment transport rates is also reflected by the model not being sensitive to $k_{s,c}$ (recall that $k_{s,c}$ affects the magnitude of the suspended sediment transport by determining the lower limit of the integral of the product of cross-shore mean-

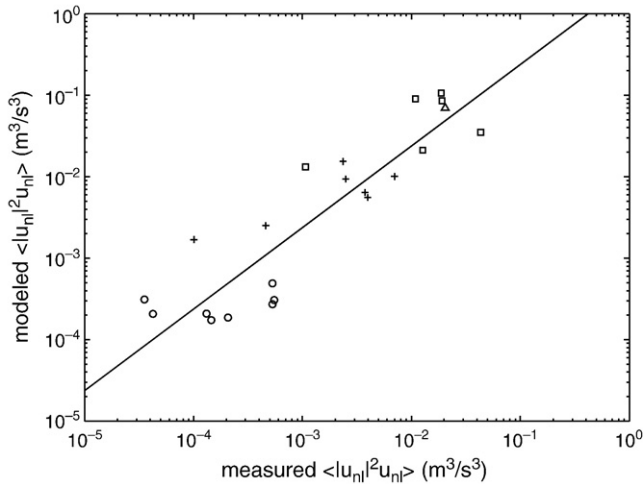


Fig. 8. Comparison between measured and modeled third-order short-wave moment $\langle |u_{ni}|^2 u_{ni} \rangle$. The correlation-coefficient squared r^2 of the best-fit line (solid line) amounted to 0.37. Symbols represent cross-shore distances: $x \approx -350$ m (circles); $x \approx -200$ m (pluses); $x \approx -155$ m (squares), and $x \approx -70$ m (triangles). Axes are log-transformed for clarity.

current and time-averaged sediment concentration). The “optimum” $k_{s,c} = 0.08$ m is therefore a non-unique value, determined by the random seed used in the generation of the 1000 parameter sets.

The model results presented in this section were obtained with a time-independent offshore wave angle of 0° . To test the sensitivity of the results to the assumption of shore-normal waves, we repeated the model calibrations with 10° and 20° angles-of-incidence. The offshore wave angle can affect model results by changing the wave height at the bar because of wave refractive effects and due to a change in bed-shear stress caused by the generation of a longshore current (e.g., Thornton et al., 1996). However, we found that these effects are not important here because about the same optimum values (and skill) for λ and $\tan \phi$ were obtained as for shore-normal waves.

4. Discussion

Although model skill is positive (0.56) at the end of the 4-day simulation period, implying that the model outperformed no-change conditions, it is obvious that the model did neither represent the rate of onshore bar migration nor the temporal evolution of the bar shape well. While the predicted onshore migration and associated reduction

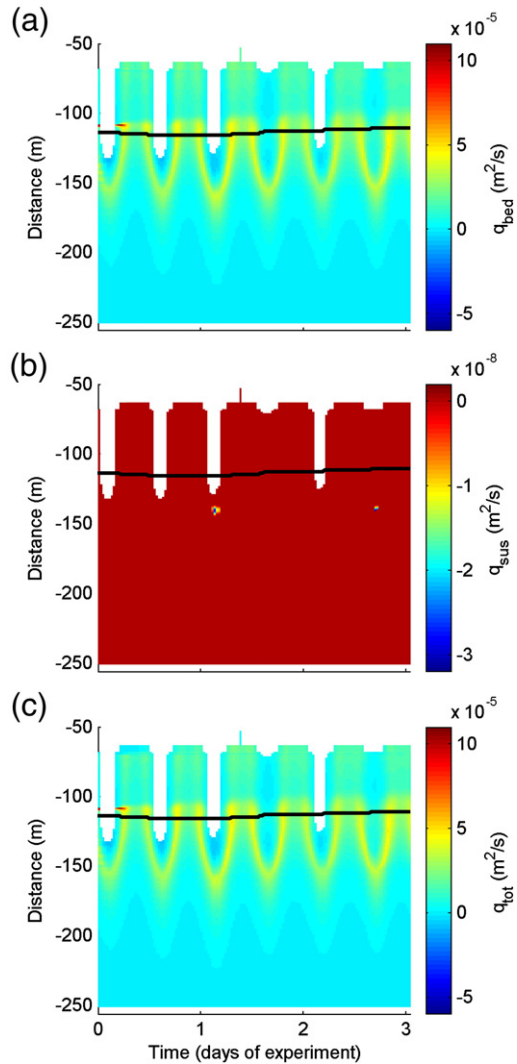


Fig. 9. Predicted (a) bedload transport rate q_{bed} , (b) suspended transport rate q_{sus} , and (c) total transport rate q_{tot} versus time. The black line represents the predicted sandbar crest location.

in bar-trough relief are consistent with observations of other subtidal sandbars (e.g., Trowbridge and Young, 1989; Plant et al., 2001), the onshore migration and simultaneous preservation of the steep, landward slipface is similar to the onshore migration of intertidal slipface ridges (e.g., Masselink et al., 2006). Fig. 5 shows that the bar crest moved predominantly onshore at low tide (e.g., about 3 m between $t=1.06$ days and $t=1.17$ days) and remained inactive at high tide (e.g., between $t=1.84$ days and $t=1.99$ days). At low tide, the water depth at the bar crest was about 0.25 m and surf zone bores were propagating across the bar (Fig. 11a). Under such circumstances the bar might be regarded as a slipface ridge, which has been observed to migrate onshore at rates exceeding 1 m/day and to retain their shape under the action of surf zone bores (Owens and Frobel, 1977; Sunamura and Takeda, 1984; Kroon, 1994). As demonstrated by Aagaard et al. (2006), under the presence of bores the onshore stroke of the wave orbital motion (and hence the associated transport capacity) is considerably stronger than the offshore stroke. The excess water transported over the bar is likely to be channelled alongshore to the nearest rip-channel (the presence of rip-channels can be deduced easily from Fig. 11b). Thus, as the bores rushed up the seaward side of the bar, sediment was transported from the seaward side of the bar towards the crest, shunting sediment into the trough. This results in accretion shoreward of the bar crest and on its slip face and, therefore, landward bar migration. These shallow-water surf zone processes are missing from the applied model and highlight a priority for further field study and model development.

Consistent with earlier work (e.g., Gallagher et al., 1998; Ruessink et al., 2007; Ruessink and Kuriyama, 2008) we used the dominance of root-mean-square over net bed level change in the measurement transect as a justification for the use of a model that ignores alongshore variability in bathymetry, waves and currents. Although the dominance of the root-mean-square change over the net change implies that sediment was predominantly redistributed in the cross-shore direction, our work demonstrates that this dominance does not imply that the bathymetry was actually alongshore uniform. In hindsight, it is surprising that despite the presence of alongshore non-uniformities in the bathymetry and missing governing processes



Fig. 11. (a) Snap-shot and (b) time-averaged video image of Tairua Beach at low tide during the experiment.

in the model we still obtained a skill of 0.56. As pointed out earlier by Hsu et al. (2006) and Ruessink et al. (2007), we cannot rule out the possibility that the tuning of the model's free parameters compensated for missing physics. This possibility also applies to other earlier work on onshore sandbar migration.

5. Conclusions

We observed the onshore migration (3.5 m/day) of a nearshore sandbar at Tairua Beach, New Zealand during 4 days of low-energy wave conditions (offshore $H_{rms} < 0.5$ m). The morphological observations, together with concurrent measurements of waves and suspended sediment concentrations, were used to test a coupled, wave-averaged, cross-shore model. Because of the coarse bed material and the relatively low-energy conditions, the contribution of the suspended transport to the total transport was predicted and observed to be negligible. The model predicted onshore bar migration primarily at high tide as a result of onshore directed (because of wave skewness) bedload transport rates. However, this result contrasts with the field observations showing that the largest onshore bar migration rates occurred at low tide, when surf zone bores in very shallow water (< 0.25 m) may have dominated the flow field. Also, the model flattened the bar, which contrasts with the steep front-face of the bar as observed during the entire experiment. Thus, our analyses of the field observations and the numerical simulations indicate that the bar behaved as an intertidal slipface ridge at low tide and as a surf zone sandbar during high tide. This would imply that onshore propagating surf zone bores in very shallow water, which are absent from the present model, play a key role in the observed sandbar behaviour. The possibility that the excess water transported by the bores across the bar was channelled alongshore to near-by rip-channels further implies

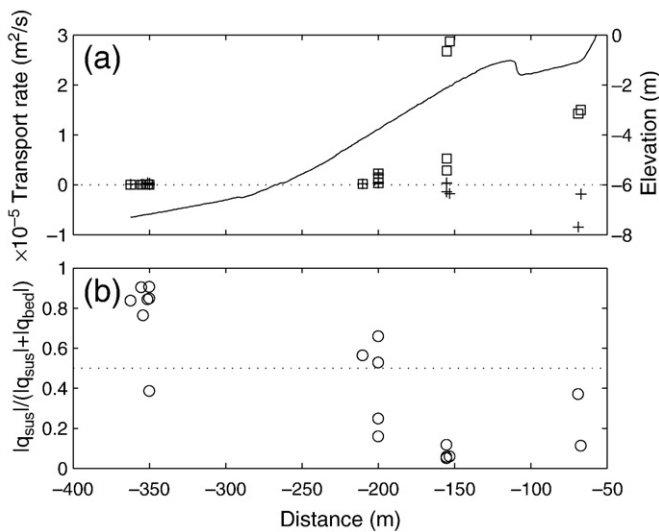


Fig. 10. (a) Predicted bedload transport rate q_{bed} (squares) and suspended transport rate q_{sus} (pluses) calculated by multiplying the predicted velocity profiles by the measured concentration profiles for multiple cross-shore locations. Variability in transport magnitudes for similar cross-shore locations is the result of measurements being taken during different conditions. (b) $|q_{sus}|/(|q_{sus}|+|q_{bed}|)$ to examine the contribution of suspended transport to the total transport. The dotted line in (a) indicates the zero transport rate and in (b) it indicates that q_{sus} and q_{bed} are of equal importance. The solid line in (a) represents the measured bed profile on March 13.

that traditional cross-shore measures to judge the applicability of a cross-shore morphodynamic model may be misleading. The obtained positive model skill (0.56) relative to a no-change model may imply that the free model parameters compensated partly for missing physics (inner surf zone bores) and/or the violation of the assumption of alongshore uniformity in morphology. This dataset, characterizing conditions typical of many other sites (Wijnberg and Kroon, 2002; Aagaard et al., 2006), provides a challenge for nearshore researchers and highlights a priority for future field studies and a foundation for the development of new models which will need to include and couple surf and swash zone processes.

Acknowledgements

Field assistance by R. Owendon, K. Smith, R. Budd, A. Swales, R. Lifting, J. Radford, and the Surf Life Saving New Zealand club of Tairua Beach is gratefully acknowledged. The video system of Tairua Beach is funded by Environment Waikato and the video system was mounted on the Homans' residence. Giovanni Coco and B.G. Ruessink funded by the (New Zealand) Foundation for Research, Science and Technology, and by the Netherlands Organisation for Scientific Research NWO (contract 864.04.007), respectively.

References

- Aagaard, T., Hughes, M., Møller-Sørensen, R., Andersen, S., 2006. Hydrodynamics and sediment fluxes across an onshore migrating intertidal bar. *J. Coast. Res.* 22, 247–259.
- Battjes, J.A., Janssen, J.P.F.M., 1978. Energy loss and set-up due to breaking of random waves. *Proc. 16th Int. Conf. on Coastal Engineering*. ASCE, New York, pp. 570–587.
- Bogle, J.A., Bryan, K.R., Black, K.P., Hume, T.M., Healy, T.R., 1999. Observations of geomorphic parameters using video images. *Coasts and Ports '99*, vol I, Proceedings of the 14th Australasian Coastal and Ocean Engineering conference and the 7th Australasian Port and Harbour Conference, April 14–16, Perth, Australia, pp. 70–75.
- Caplan, P., Derber, J., Gemmil, W., Hong, S.-Y., Pan, H.-L., Parish, D., 1997. Changes to the 1995 NCEP operational medium-range forecast model/analysis/forecast system. *Weather Forecast.* 4, 335–343.
- Falchetti, S., Brocchini, M., Conley, D.C., 2007. Sediment transport and underwater bar migration. In: Dohmen-Janssen, Hulscher (Eds.), *Proceedings of River, Coastal and Estuarine Morphodynamics: RCEM2007*. Taylor & Francis Group, London, pp. 583–589.
- Gallagher, E.L., Elgar, S., Guza, R.T., 1998. Observations of sand bar evolution on a natural beach. *J. Geophys. Res.* 103 (C2), 3203–3215.
- Garnier, R., Calvete, D., Falques, A., Caballeria, M., 2006. Generation and nonlinear evolution of shore-oblique/transverse sand bars. *J. Fluid Mech.* 567, 327–360.
- Henderson, S.M., Allen, J.S., Newberger, P.A., 2004. Nearshore sandbar migration predicted by an eddy-diffusive boundary layer model. *J. Geophys. Res.* 109 (C06024). doi:10.1029/2003JC002137.
- Hoefel, F., Elgar, S., 2003. Wave-induced sediment transport and sandbar migration. *Science* 299, 1885–1887.
- Hsu, T.J., Elgar, S., Guza, R.T., 2006. Wave-induced sediment transport and onshore sandbar migration. *Coast. Eng.* 53, 817–824.
- Kroon, A., 1994. *Sediment Transport and Morphodynamics of the Beach and Nearshore Zone near Egmond, The Netherlands*. PhD thesis, Utrecht University.
- Masselink, G., Kroon, A., Davidson-Arnott, R.G.D., 2006. Morphodynamics of intertidal bars in wave dominated coastal settings — a review. *Geomorphology* 73, 33–49.
- Nairn, R.B., Roelvink, J.A., Southgate, H.N., 1990. Transition zone width and implications for modelling surfzone hydrodynamics. *Proc. 22nd Int. Conf. on Coastal Engineering*. ASCE, New York, pp. 68–82.
- Nielsen, P., 1979. *Some Basic Concepts of Wave Sediment Transport*. Series Paper No 20. Institute of Hydrodynamics and Hydraulics Engineering, Technical University of Denmark. 160 pp.
- Owens, E.H., Frobel, D.H., 1977. Ridge and runnel systems in the Magdalen Islands, Quebec. *J. Sediment. Petrol.* 47, 191–198.
- Plant, N.G., Freilich, M.H., Holman, R.A., 2001. Role of morphologic feedback in surf zone sandbar response. *J. Geophys. Res.* 106, 973–989.
- Plant, N.G., Holland, K.T., Puleo, J.A., Gallagher, E.L., 2004. Prediction skill of nearshore profile evolution models. *J. Geophys. Res.* 109 (C01006). doi:10.1029/2003JC001995.
- Reniers, A.J.H.M., Thornton, E.B., Stantio, T.P., Roelvink, J.A., 2004. Vertical flow structure during Sandy Duck: observations and modeling. *Coast. Eng.* 51, 237–260. doi:10.1016/j.coastaleng.2004.02.001.
- Ribberink, J.S., 1998. Bed-load transport for steady flows and unsteady oscillatory flows. *Coast. Eng.* 34, 59–82.
- Rienecker, M.M., Fenton, J.D., 1981. A Fourier approximation for steady water waves. *J. Fluid Mech.* 104, 119–137.
- Roelvink, J.A., Meijer, T.J.G.P., Houwman, K., Bakker, R., Spanhoff, R., 1995. Field Validation and Application of a Coastal Profile Model. *Proceedings of Coastal Dynamics*, vol. 95. ASCE, New York, pp. 818–828.
- Ruessink, B.G., Kuriyama, Y., 2008. Numerical predictability experiments of cross-shore sandbar migration. *Geophys. Res. Lett.* 35 (L01603). doi:10.1029/2007GL032530.
- Ruessink, B.G., Kuriyama, Y., Reniers, A.J.H.M., Roelvink, J.A., Walstra, D.J.R., 2007. Modeling cross-shore sandbar behaviour on the time scale of weeks. *J. Geophys. Res.* 112 (F03010). doi:10.1029/2006JF000730.
- Smith, R.K., Latimer, G.J., Swales, A., Rutherford, J.C., Budd, R.G., Owendon, R., Hambling, J., 1997. Nearshore profile and bedform measurements using an enhanced sea sled survey technique. *Shore Beach* 65 (4), 15–24.
- Sunamura, T., Takeda, I., 1984. Landward migration of inner bars. *Mar. Geol.* 60, 63–78.
- Thornton, E.B., Humiston, R.T., Birkemeier, W., 1996. Bar-trough generation on a natural beach. *J. Geophys. Res.* 101, 12097–12110.
- Trowbridge, J., Young, D., 1989. Sand transport by unbroken water waves under sheet flow conditions. *J. Geophys. Res.* 94, 10971–10991.
- Van Rijn, L.C., 1993. *Principles of Sediment Transport in Rivers, Estuaries and Coastal Seas*. Aqua Publications, Amsterdam.
- Van Rijn, L.C., 1995. Yearly averaged sand transport at the 20 m and 8 m NAP depth contours of the JARKUS profiles 14, 40, 76 and 103. Report h1887, Delft Hydraulics.
- Wijnberg, K.M., Kroon, A., 2002. Barred beaches. *Geomorphology* 48, 103–120.
- Wright, L.D., Short, A.D., 1984. Morphodynamic variability of surf zones and beaches: a synthesis. *Mar. Geol.* 56, 93–118.